

# How fast can fluids squeeze through micro-pores?

Tom Chou

DAMTP, Cambridge University, Cambridge CB3 9EW, ENGLAND

We use a one dimensional symmetric exclusion model to study pressure and osmosis driven flows through molecular-sized channels, such as biological membrane channels and zeolite pores. Analytic expressions are found for the steady-state flow which show rich nonlinear behavior. We find a maximum in the flow rates depending upon pore radius, pore energetics, reservoir temperature, and driving force. We also present exact mean-field results of transport through pores with internal defects. The interesting nonlinear dependences suggest numerous diagnostic experiments in biological and zeolitic systems which may reveal the features presented.

The answer to the title question is tremendously important in analyzing biological and industrial processes, and has received recent attention with the finding that tracer particle motions in a micro-pore are governed by subdiffusive dynamics [1]. Biological examples include membranes containing molecular-sized channels specific to water transport which participate in cellular volume regulation controlled by hydrostatic or osmotic pressure [2,3]. Classes of biological ion channels have also been demonstrated to be pores of molecular size [2,3]. Man-made materials such as zeolites and carbon nanotubes also contain many microscopic, statistically nearly single-file channels which can selectively absorb fluids. This size specificity can be exploited in separation of a mixture of linear and branched chain alkanes, where the zeolite acts as like a sponge absorbing only the desired specie(s) [4]. Confining particles in zeolite pores can also serve to catalyze reactions: How fast can one get reagents into micro-pores and the products out? Therefore, the design and manufacture of porous materials is an economically motivated area of research. Not surprisingly, vast amounts of numerical simulation have been performed on a variety of specific systems [5].

Confined particles are strongly interacting due to excluded volume [1,6] as shown in recent NMR and theoretical studies [1]. Anomalies in numerically computed (MD) “diffusion” constants have been found [7]. However, numerical simulations neither access the long time scales required to study steady state flow, nor offer a unifying physical picture of the parameter regimes important for transport. To obtain reasonable flow rates using MD, artificial external forces such as gravity are often imposed [8,9]; in 1D systems such external forces can yield qualitatively different behavior (such as shock profiles) from osmosis and pressure driven flow [10], which occur in the absence of such intrinsic forces.

A model of micro-flow that physically describes microscopic transport and how it depends on macroscopic experimental parameters would serve as a useful benchmark in more sophisticated models and complement more detailed MD simulations. Consider the molecular-sized pore shown in Fig. 1, with particles driven from (L) to (R) either by osmotic “pressure”  $\Delta\Pi$ , or by hydro-

static pressure  $\Delta P$ . The pore is divided into sections  $i$  of length  $\ell$ . Enthalpic energy differences between bulk and sectioned pore particles are shown, as well as possible activation barriers. Entrance(exit) rates at the left and right boundary sites are denoted by  $\alpha(\gamma)$  and  $\delta(\beta)$  respectively. Here,  $\alpha dt$  and  $\delta dt$  are the probabilities for pore entry in time  $dt$  *only if* the occupations  $\tau_{i=1} = 0$  and  $\tau_{i=N} = 0$  respectively. The probability per unit time a randomly picked interior particle moves one section to the right(left) is  $p(q)$  *only if* the site to the right(left) is unoccupied.

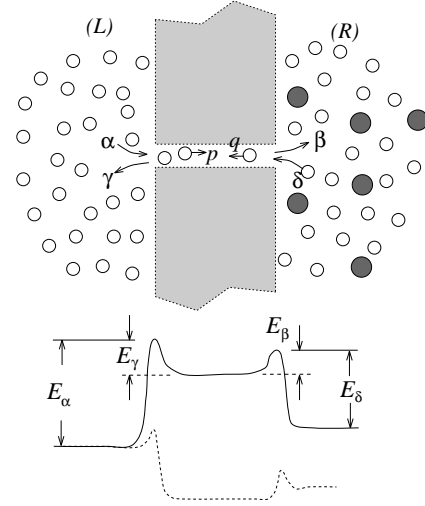


FIG. 1. Schematic of osmosis and pressure driven flow through membrane pores separating infinite reservoirs (L) and (R). The coefficients  $\alpha, \beta, \gamma, \delta$  are conditional solvent entrance and exit probabilities at pore ends.

The assumption of no pass pores is accurate even for pores with diameters few times that of the particles: Overtaking requires a restricted subset of geometries and will be statistically rare. Even when overtaking occurs, interchange between particles at sites  $i$  and  $i+1$  does not contribute to net flux. Although our treatment is rigorous for no pass pores, it is accurate as long as the average number of particles in a cylindrical slice of length  $\ell$  is  $\lesssim 1$ . Consider the instantaneous number flux between sections  $i$  and  $i+1$ ,

$$\begin{aligned}
J(t) &= p\tau_i(t)(1 - \tau_{i+1}(t)) - q\tau_{i+1}(t)(1 - \tau_i(t)) \\
&= p(\tau_i(t) - \tau_{i+1}(t)) + \epsilon\tau_{i+1}(t) - \epsilon\tau_i(t)\tau_{i+1}(t).
\end{aligned} \tag{1}$$

Although much attention has focussed on the asymmetric exclusion model, particularly in the thermodynamic limit, where many exact results are known [10], the symmetric exclusion model is valid in the absence of external electric or gravitational forces,  $\epsilon = p - q = 0$ . This reveals that hydraulic and osmotic pressure driven flows through microscopic pores are simply a consequence of a density gradient which induces particles to directionally or cooperatively diffuse; however, locally, a particle is as likely to move to the left or right *if* both left and right adjacent sites are unoccupied. The random updating in particle motions implicit in the model dynamics is clearly valid in systems where long wavelength collective modes are irrelevant.

Linearity of  $J(t)$  when  $\epsilon = 0$  renders the mean-field steady state current  $J$  found from time averaging Eq. (1) exact. Steady state particle conservation along the pore length results in a linear density profile  $J = p(\tau_1 - \tau_N)/(N - 1)$ ; this, along with the steady state boundary conditions  $J_1 = J = \alpha(1 - \tau_1) - \gamma\tau_1$  and  $J_N = J = \beta\tau_N - \delta(1 - \tau_N)$ , determine the steady state particle number flux

$$J(N) = \frac{p(\alpha\beta - \gamma\delta)}{(N - 1)(\alpha + \gamma)(\beta + \delta) + p(\alpha + \beta + \gamma + \delta)}. \tag{2}$$

The kinetic parameters  $\{\mu\} \equiv (\alpha, \beta, \gamma, \delta)$  are related to the *relative* enthalpies of activation  $E_\mu$  between pore and bath particles. We assume local thermodynamic equilibrium (LTE), particularly valid in liquid phase osmosis across single biological pores where  $J \leq 10^9/\text{s}$ , typical pore diameters and interparticle spacings  $\lambda \sim 5\text{\AA}$ , and ambient thermal velocities  $v_T \simeq 4 \times 10^4 \text{cm/s}$ , yield collision times  $t_{\text{coll}} \simeq \lambda/v_T \simeq 1\text{ps} \ll J^{-1}$ . Therefore, particles suffer  $O(10^3)$  collisions before they are osmotically transported, sufficient for (LTE). As an illustrative example, we consider an axisymmetric right cylindrical pore. The kinetic parameters under LTE will be defined by simple transport theory,

$$\begin{aligned}
p &\approx (v_T/\ell) \exp(-E_p/k_B T); \quad \beta \approx (v_T/\ell) \exp(-E_\beta/k_B T) \\
\alpha &\equiv \alpha_0 \exp(-E_\alpha/k_B T) \approx \frac{1}{4} n_L v_T (\pi r_p^2) \exp(-E_\alpha/k_B T)
\end{aligned} \tag{3}$$

where  $v_T \sim \sqrt{k_B T/m}$  is the thermal velocity,  $\ell$  is chosen to be the minimum statistical spacing between pore particles, and  $n_L$  is the number density in the left reservoir. The minimum particle spacing  $\ell$  can be estimated for each set of  $\{\mu\}$  from a 1D Tonk's gas [11]. Since we explore considerable variations in  $\{\mu\}$ , we choose  $\ell \sim a$ , approximately a hard core repulsive diameter; thus,  $p$  given in (3) represents a ballistic travel time over the distance  $\ell \simeq a$ , weighted by an energetic binding  $E_p$ .

A larger choice for  $\ell$  can be made if  $(\ell/a)\tau_i < 1$  and with  $p$  appropriately rescaled and entropic factors included for  $\{\mu\}$  (the  $E_\mu$  are then effective free energies); this is useful in multiple species models where steady state flows for long pores cannot be obtained analytically [12]. Note that for  $\ell \gg a$ , *local* free diffusive transport described by  $p \simeq \ell^{-2}$  may obtain. But when  $\ell \simeq a$ ,  $E_\mu$  represent enthalpies determined entirely by molecular potentials. Thus,  $E_\alpha(r \leq r_p) - E_\alpha(0) \lesssim k_B T$  (where  $E_\alpha(r = 0) \equiv E_\alpha$ ) defines an effective pore radius  $r_p$ . For pores that repel particles (top curve in Fig. 1) and have negligible activation energies  $E_\beta$  and  $E_p$ ,  $p/\beta \sim O(1)$ .

Further simplification is gained by considering microscopically symmetric pores where  $\beta = \gamma$ , and normalizing (denoted by an overbar) all quantities by  $\beta$  (such that  $\bar{J} = 1$  would be the maximum flow rate possible, when  $\tau_N = 1$ ) so that

$$\bar{J}(N) = \frac{\bar{\alpha}\bar{p}\Delta}{(N - 1)(\bar{\alpha} + 1)(\bar{\alpha} + 1 - \bar{\alpha}\Delta) + \bar{p}(2\bar{\alpha} + 2 - \bar{\alpha}\Delta)}, \tag{4}$$

where

$$\Delta = 1 - e^{\Delta E/k_B T} + \frac{\Delta n_{\text{solute}}}{n_L} e^{\Delta E/k_B T} \tag{5}$$

and  $\Delta E \equiv E_\alpha - E_\delta(P_R - P_L)$ . Eqn. (5) represent differences in number density and/or enthalpies between (R) and (L) and along with (4) determine the flow through symmetric pores. In osmotic flow under isobaric conditions,  $\Delta E = 0$ , in pressure driven flow of nearly ideal gases,  $(\partial \Delta E / \partial P_R)_T \simeq 0$ , while pressure driven flows of liquids is described by  $(\partial n_R / \partial P)_T \simeq 0$ . In the first two cases, the flux is predominately the consequence of increased permeable particle density in one of the reservoirs over the other, while pressure driven flow of liquids results mainly from the relative reduction of pore entrance activation energies brought about by hydrostatic compression. We first consider fixed  $\Delta = 0.02$  which corresponds to an osmotic pressure in aqueous solution of  $\Delta \Pi \simeq 25 \text{atm}$  or a hydrostatic pressure difference of  $\Delta P \simeq 0.025 \text{atm}$  of gas at STP. Using the Maxwell relationship for molar volume,  $-(\partial \Delta E / \partial P_R)_T \simeq \bar{v}$ , we find  $\Delta = 0.02$  also corresponds to  $P_R - P_L \simeq 25 \text{atm}$  in pressure driven flow of water at 300K.

When  $\bar{\alpha}\Delta/(\bar{\alpha} + 1)$  is negligible, flows are essentially linear in  $\Delta$  and defined by hydraulic or osmotic permeabilities,  $J = L_p \Delta P$  or  $J = P_{os} \Delta \Pi$ . Although  $L_p$  and  $P_{os}$  have often been, and continue to be interpreted using macroscopic fluid mechanics [3], a microscopic description arises here. In the limit  $\bar{p} \gg (\bar{\alpha} + 1)N$ , rate limiting steps involve pore entrance or exit. Linearizing (5) and (4), we find

$$L_p = \frac{\alpha}{2(\bar{\alpha} + 1)k_B T} \left( \frac{\partial \Delta E}{\partial P_R} \right)_T \tag{6}$$

for pressure driven flow of dense liquids. The temperature dependence of  $L_p$  will be determined by  $-E_\beta/k_B T$  [ $-E_\alpha/k_B T$ ] for  $\bar{\alpha} \gg 1$  [ $\bar{\alpha} \ll 1$ ] if the thermal coefficient of expansion  $\approx 0$ . When  $\bar{p} \ll (\bar{\alpha} + 1)N$ ,

$$L_p = \frac{\bar{\alpha}\bar{q}}{(N-1)(\bar{\alpha}+1)^2 k_B T} \left( \frac{\partial \Delta E}{\partial P_R} \right)_T \quad (7)$$

which has a  $(E_\alpha - E_\beta - E_p)/k_B T$  [ $(E_\beta - E_\alpha - E_p)/k_B T$ ] Arrhenius temperature dependence for  $\bar{\alpha} \gg 1$  [ $\bar{\alpha} \ll 1$ ]. Note that the  $\bar{\alpha} \gg 1$  regime of (7) yields a curious  $L_p \propto r_p^{-2}$  dependence. In the limit where (7) holds, the bottlenecks occur in the particle motions within the pore interior. Expressions for  $L_p$  of ideal gases and  $P_{os}(P_L = P_R)$  are found from (6) and (7) by replacing  $(\partial \Delta E / \partial P_R)_T \rightarrow \mp n_L^{-1}$  respectively in the corresponding limits; the temperature dependences remain unchanged. Values of all energetic barriers mentioned above are qualitatively consistent with osmotic flow through biological pores where hydrogen bonds ( $E_\alpha \sim 10k_B T$  in the  $\bar{\alpha} \ll 1$  limit of (7)) must be broken before water can enter.

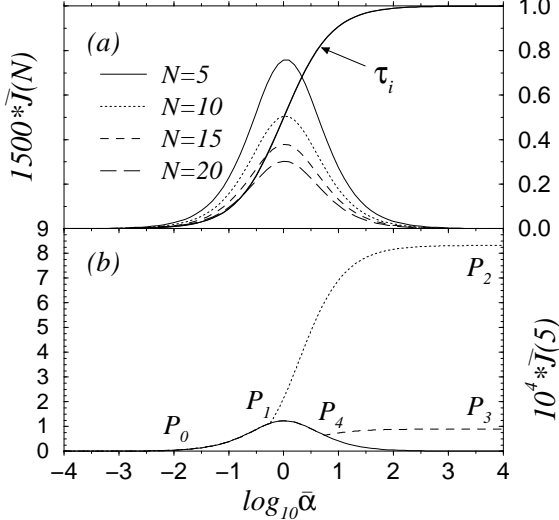


FIG. 2. (a)  $1.5 \times 10^3 \bar{J}(N, \bar{\alpha})$  for  $\Delta = 0.02$  and fixed  $\bar{p}_0 = 1.0$ . Various lengths are indicated. The solid curve between 0 and 1 is the average occupation number of any site. On this scale, the difference  $\tau_1 - \tau_N$  is not apparent but varies qualitatively as  $\bar{J}$ . (b) The solid curve is  $10^4 \times \bar{J}(5)$  for fixed  $\bar{p}_0 = 0.1$ . See text for explanation of curves  $P_0 P_1 P_2$  and  $P_0 P_1 P_4 P_3$ .

The solid curve in Figure 2(a) shows  $(1.5 \times 10^3) \times \bar{J}(N)$  (from Eq. (4)) for  $\bar{p} = 1$ ,  $\Delta = 0.02$  for various pore lengths  $N \simeq L/a$ . We find a maximum flux  $\bar{J}^*$  at

$$\bar{\alpha}^* = \left[ \frac{2\bar{p}_0 + (N-1)}{(N-1)(1-\Delta)} \right]^{1/2} \quad (8)$$

for fixed  $\bar{p} = \bar{p}_0$ . The maximum occurs because at intermediate occupancies, the pore is conducting a significant number of particles, but is not yet choked off.

Large values of  $\bar{\alpha}$  represent pores which are attractive to the solvent, depicted by the dashed energy landscape in Fig. 1. As the pore is made increasingly attractive  $E_\beta > 0$ , and  $\beta$  must eventually diminish so that  $\bar{p} = p/\beta \propto \exp[(E_\beta - E_p)/k_B T]$ . However, we will explicitly show that the maximum at  $\bar{J}^*$  can persist. Assume no activation barriers at the pore mouths, *ie.*,  $E_\beta(E_\alpha) = 0$  for  $E_\alpha(E_\beta) > 0$  and consider molecularly repelling pores where  $0 < \bar{\alpha} < \bar{\alpha}_0$  ( $E_\alpha > 0$ ,  $E_\beta = 0$ ); here,  $\bar{p} \approx \exp(-E_p/k_B T)$ , independent of the pore energy level. As the pore is made attracting,  $\bar{p}$  will acquire  $\exp(E_\beta/k_B T)$  behavior and can be defined as

$$\bar{p} = \bar{p}_0 \left[ \frac{\bar{\alpha}}{\bar{\alpha}_0} \theta(\bar{\alpha} - \bar{\alpha}_0) + \theta(\bar{\alpha}_0 - \bar{\alpha}) \right]. \quad (9)$$

where  $\theta(x > 1) = 1$  is the Heaviside function indicating when the pore first becomes molecularly attracting. Using (9),  $\bar{J}(N, \bar{\alpha} \rightarrow \infty)$  (the current in the limit of infinitely attracting pores) becomes

$$\bar{J}^\infty(N) = \frac{\bar{p}_0 \Delta}{\bar{\alpha}_0(N-1)(1-\Delta) + \bar{p}_0(2-\Delta)}, \quad (10)$$

which can approach  $\Delta/(2-\Delta) > \bar{J}^*$ . For  $\bar{\alpha}_0 \gg \bar{\alpha}^*$ , the maximum remains at  $\bar{\alpha}^*$ . However, when  $\bar{\alpha}_0 \lesssim \bar{\alpha}^*$ ,  $\bar{\alpha}$ ,  $\bar{p} \approx \exp(E_\beta/k_B T)$  and the maximum in flux as a function of  $\bar{\alpha}$  is preempted by a current which approaches (10). The condition for  $\bar{J}^\infty(N) < \bar{J}^*(N)$  (a remaining maximum in  $\bar{J}$  as pore well depth is increased) is determined by

$$\bar{\alpha}_0 > \bar{\alpha}^* + \frac{\bar{\alpha}^{*2}}{\bar{\alpha}^* + 1} \quad (11)$$

Fig. 2(b) compares the behavior of  $10^4 \times J(5)$  using  $\bar{p} = \bar{p}_0 = 0.1$  (solid curve) with that of  $10^4 \times J(5)$  using Eq. (9) (broken lines). For  $\Delta = 0.02$ , the maximum at  $\bar{\alpha}^* = \sqrt{15/14}$  is destroyed when (11) is satisfied,  $\bar{\alpha}_0 \lesssim 1.562$ . Estimating  $\bar{\alpha}_0$  from (3) and  $\Delta = 0.02$ ,  $\bar{\alpha}_0 \ll \bar{\alpha}^*$  for gases, but can be  $O(1)$  for liquids. Curve  $P_0 P_1 P_4 P_3$  retains the maximum  $\bar{J}^*$  since  $\bar{\alpha}_0 = 10^{0.75} > 1.562$ , while  $P_0 P_1 P_2$  corresponds to  $\bar{\alpha}_0 = 10^{-0.25} < 1.562$  which gives a monotonic  $J$  as  $\bar{\alpha} \rightarrow \infty$ . A high current may occur at  $\bar{\alpha} \rightarrow \infty$  despite the high pore occupancy due to an accompanying exponential increase in  $\bar{p}$ . As expected, these high values are more difficult to achieve as  $\bar{\alpha}_0$  (as well as  $N$ ) increases, because the onset of exponentially increasing  $\bar{p}$  is delayed.

Now consider the nonlinear effects of large  $\Delta$ . According to (8), values of  $\bar{\alpha}$  that give a maximal  $\bar{J}^*$  depend strongly on  $\Delta$ ; thus,  $\Delta \rightarrow 1$  can yield large  $\bar{\alpha}^* \gg \bar{\alpha}_0$  where the maximum in flux is destroyed. At the maximum value  $\Delta = 1$  (corresponding to approximately to pure solute or vacuum in  $(R)$ ), the maximum flux occurs when  $\bar{p} \gg N$  and approaches  $\bar{J}(\Delta = 1) \simeq \bar{\alpha}/(\bar{\alpha} + 2)$ . The smallest flux occurs when  $\bar{p} \ll N$  and  $\bar{\alpha} \ll 1$  as

expected. The nonlinearity of  $\bar{J}(\Delta)$  is important only when  $\bar{\alpha} \gg 1$ , as shown in Figure 3, corresponding to a pore interior with high particle occupation, when particle exclusion nonidealities are most pronounced.

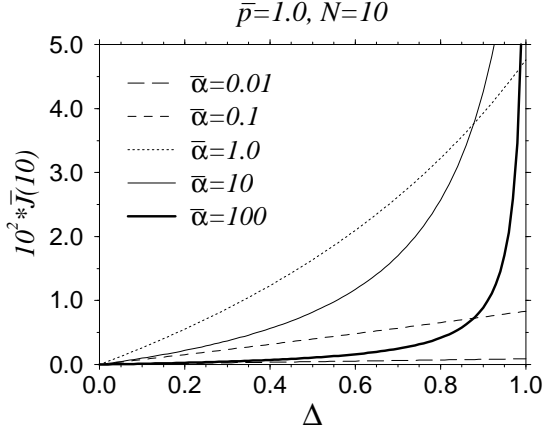


FIG. 3. Nonlinear behavior of  $10^2 \times \bar{J}(10)$  for  $\bar{p} = 1.0$  as a function of  $\bar{\alpha}$ . Note the competition between nonlinearities in  $\bar{\alpha}$  and  $\Delta$ , particularly at large  $\Delta$ .

To experimentally test possible nonlinearities densities, pressures, and temperatures may need to be substantially varied, and is readily performed only in zeolite systems. Adiabatic ultrasonic driving with frequency  $\omega \ll J^{-1}$  of the fluid in  $(R)$  (not affecting  $\bar{\alpha}$  which depends only on  $n_L$ ) will enhance transport: Upon setting  $\Delta(t) = \Delta_0 + \Delta_1 \cos \omega t$  and averaging over a period,

$$\bar{J}(N) = \bar{J}(N, \Delta_1 = 0) + \frac{\bar{J}(N, \Delta_1 = 0)}{2} \times \left\{ \begin{array}{ll} \frac{\bar{\alpha}^2 \Delta_1^2}{\bar{\alpha}(2 - \Delta_0) + 1} & \bar{p} \gg (\bar{\alpha} + 1)N \\ \frac{\Delta_1^2}{(1 - \Delta_0)^2} & \bar{p} \ll (\bar{\alpha} + 1)N \end{array} \right\} + O(\Delta_1)^3 \quad (12)$$

for small  $\Delta_1/\delta_0$ . In the  $\bar{p} \gg (\bar{\alpha} + 1)N$  case, the temperature dependence of the flux enhancement is  $-2E_\alpha/k_B T$  or  $-E_\alpha/k_B T$ , while the second case is temperature independent.

Effects of microscopic internal pore structure/disorder on microflow can also be modelled. Consider  $N^*$  defects in hopping rates  $p_k^*(t) = q_k^*(t)$ , between sections  $i(k)$  and  $i(k) + 1$ . When  $p_k^*(t)$  is statistically independent of  $\tau_i(t)$ , the mean-field result

$$J = \frac{p(\alpha\beta - \gamma\delta)}{(\alpha + \gamma)(\beta + \delta)(N - 1 + \Omega) + p(\alpha + \beta + \gamma + \delta)}, \quad (13)$$

where  $\Omega \equiv \sum_{k=1}^{N^*} (p/p_k^* - 1)$ , is exact. Biological and zeolitic channels contain internal pore structure exposing random binding sites  $E_p(k)$ . An example of a one-defect pore is gramicidin A channels across a biomembrane. These are composed of two barrel structures,

one in each lipid layer, joined by attractive molecular interactions near the bilayer midplane forming a defect bisecting the entire channel. Osmosis experiments on Gramicidin A/bilayer liposomes reveal rich temperature dependences which are interpreted as lipid phase transitions inducing changes in how the Gramicidin A barrels are joined [13]. Molecular permeation through pure lipid bilayers is also modelled by (13). Biolipid head-groups offer activation barriers such as those depicted in Fig 1. Within the hydrophobic lipid tails, particle motions are predominantly perpendicular to the membrane along the aliphatic chains. Thus, bilayer membranes physically resemble many close-packed channels with defects at the bilayer midplane, where the ends of the hydrocarbon chains approach each other, and at stiff unsaturated bonds along the fatty acid chains. Various zeolites are comprised of interconnected cages and joints which are also modelled using (13), although actual flow measurements are ensemble averages over macroscopic membrane regions containing many pores:  $\langle \bar{J} \rangle = \sum_{N, N^*, p^*} f(N, N^*, p_k^*) \bar{J}(N, N^*, p_k^*)$ , where  $d$  is the membrane thickness,  $N_{min} \simeq d/\ell$ , and  $f(N, N^*, p_k^*)$  is the distribution of channels with arc-length  $L = N/\ell$ , number of defects  $N^*$ , and defect strengths  $p_k^*$ . We mention that the steady state result (13) is also an exact solution to the Heisenberg spin chain hamiltonian with boundary conditions determined by  $\{\mu\}$  and quenched random energies [14].

Since the particle density at section  $i$  obeys  $\dot{\tau}_i = q(\tau_{i+1} - 2\tau_i + \tau_{i-1})$  which on scales  $\gg \ell$  is a diffusion equation with  $q\ell^2$  defining a cooperative diffusion coefficient, osmosis occurs strictly by mass diffusion, different from tracer diffusion. Conditions required for a maximum in  $J(\bar{\alpha})$  depend on the pre-exponential factor  $\alpha_0$  for realistically defined  $\{\mu\}$ . In LTE, relationships among the various kinetic parameters and various fluids can be determined by equilibrium measurements such as solvent-solute volumes and heats of mixing. The different Arrhenius temperature regimes delineated may also be simple way of systematically probing solvent-pore interactions. Experimentally the nonlinearities in  $\Delta$  may be probed by low frequency acoustic driving. Electrostriction and mechanical deformation of the pores may also control  $\bar{\alpha}$  and  $p$  via  $r_p$  [7]. Effects of unstirred layers near the pore mouths can be easily treated with macroscopic convection-diffusion equations, but are experimentally [3] and theoretically [12] found to be unimportant in aqueous osmosis. When important, unstirred layers yield an implicit equation  $J \propto \Delta(J)$  [12]. The simple model presented along with the numerous applicable physical systems and proposed experimental tests complements MD simulations and will subsequently lead to a better understanding of more complex systems, including multispecies transport and chemical reactions in pores.

- 
- [1] V. Gupta, S. S. Nivarthi, A. V. McCormick, H. T. Davis, Chem. Phys. Lett., **247**, 596, (1995); K. Hahn, J. Kärger, and V. Kukla, Phys. Rev. Lett., **76**(15), 2762-2765, (1996); C. Rödenbeck, J. Kärger, and K. Hahn, Phys. Rev. E., **55**(5), 5697, (1997).
  - [2] B. Alberts, D. Bray, and J. Lewis, *Molecular Biology of the Cell*, (Garland, New York, 1994); C. H. van Os, P. Deen, J. A. Dempster, Biochim. Biophys. Acta, **1197**, 291-309, (1994).
  - [3] A. Finkelstein, *Water Movement Through Lipid Bilayers, Pore, and Plasma Membranes*, (Wiley-Interscience, New York, 1987).
  - [4] R. M. Barrer, *Zeolites and Clay Minerals as Sorbents and Molecular Sieves*, (Academic Press, London, 1978).
  - [5] S. Murad, Adsorption, **2**, 95 (1996); S. Murad, J. G. Powles and B. Holtz, Mol. Phys., **8**(6) 1473 (1995); J. M. D. MacElroy and S. H. Suh, J. Chem. Phys., **106**(20), 8595, (1997).
  - [6] T. Chou, *Phase Transitions in Confined Geometries*, Ph.D. Thesis, Department of Physics, Harvard University, 1995.
  - [7] S. Yashonath and P. Santikary, J. Phys. Chem., **98**, 6338, (1994); S. Nivarthi, A. V. McCormick, H. T. Davis, Chem. Phys. Lett., **229**, 297, (1994); V. Kukla, J. Kornatowski, D. Demuth, I. Girnus, H. Pfeifer, L. Rees, S. Schunk, K. Unger, J. Kärger, Science, **272**, 702, (1996).
  - [8] J. Koplik, J. R. Banavar, and J. F. Willemsen, Phys. Fluids A, **1**(5), 781, (1989); S. Sokolowski, Molecular Phys., **75**(6), 1301, (1992).
  - [9] R. F. Cracknell, D. Nicholson, and N. Quirke, Phys. Rev. Lett., **74**(13), 2463-2466, (1995).
  - [10] R. B. Stinchcombe and G. M. Schültz, Phys. Rev. Lett., **75**, 140, (1995); *Nonequilibrium Statistical Mechanics in One Dimension*, ed. V. Privman, (Cambridge University Press, 1997).
  - [11] H. T. Davis, J. Chem. Phys., **93**, 4339, (1990); J. Piasecki and L. Peliti, J. Phys. A, **26**, 4819, (1993).
  - [12] T. Chou, To be published.
  - [13] B. A. Boehler, J. de Gier, L. L. M. van Deenen, Biochimica et Biophysica Acta, **512**, 480-488, (1978).
  - [14] S. Sadow, Phys. Rev. E, **50**, 2660, (1994).